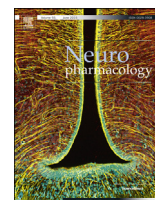




Contents lists available at ScienceDirect

Neuropharmacology

journal homepage: www.elsevier.com/locate/neuropharm

Invited review

Tracking individual membrane proteins and their biochemistry: The power of direct observation

Adam O. Barden^a, Adam S. Goler^a, Sara C. Humphreys^a, Samaneh Tabatabaei^a,
Martin Lochner^b, Marc-David Ruepp^b, Thomas Jack^b, Jonathan Simonin^b,
Andrew J. Thompson^c, Jeffrey P. Jones^a, James A. Brozik^{a,*}

^a Department of Chemistry, Washington State University, PO Box 644630, Pullman, WA, 99164-4630, United States^b Department of Chemistry and Biochemistry, University of Bern, Freiestrasse 3, CH-3012, Bern, Switzerland^c Pharmacology Department, Cambridge University, Tennis Court Road, Cambridge, CB2 1PD, United Kingdom

ARTICLE INFO

Article history:
Available online xxx

Keywords:
Single molecule fluorescence imaging
Protein tracking
P2X1
5HT3
Fluorescence
LGIC
Ligand-gated ion channel
GPCR G-protein coupled receptor
Molecular machine
Stochastic

ABSTRACT

The advent of single molecule fluorescence microscopy has allowed experimental molecular biophysics and biochemistry to transcend traditional ensemble measurements, where the behavior of individual proteins could not be precisely sampled. The recent explosion in popularity of new super-resolution and super-localization techniques coupled with technical advances in optical designs and fast highly sensitive cameras with single photon sensitivity and millisecond time resolution have made it possible to track key motions, reactions, and interactions of individual proteins with high temporal resolution and spatial resolution well beyond the diffraction limit. Within the purview of membrane proteins and ligand gated ion channels (LGICs), these outstanding advances in single molecule microscopy allow for the direct observation of discrete biochemical states and their fluctuation dynamics. Such observations are fundamentally important for understanding molecular-level mechanisms governing these systems. Examples reviewed here include the effects of allostery on the stoichiometry of ligand binding in the presence of fluorescent ligands; the observation of subdomain partitioning of membrane proteins due to microenvironment effects; and the use of single particle tracking experiments to elucidate characteristics of membrane protein diffusion and the direct measurement of thermodynamic properties, which govern the free energy landscape of protein dimerization. The review of such characteristic topics represents a snapshot of efforts to push the boundaries of fluorescence microscopy of membrane proteins to the absolute limit.

This article is part of a Special Issue entitled 'Fluorescent Neuro-Ligands'.

© 2015 Published by Elsevier Ltd.

1. Introduction

1.1. The power of direct observation and the promise of single molecule experiments

Experimental biology is a discipline that relies on direct observation and ample measurements to impart statistical relevance. New advances in single molecule fluorescence imaging promise to bring that experimental approach to the single protein level by allowing for the direct observation of (1) the way proteins move and interact with one another, (2) the binding and unbinding of

small molecules, (3) the stochastic kinetic rates that arise from different conformational manifolds, (4) the distribution of discrete states in small ensembles of individually tracked proteins, and (5) individual chemical reactions arising from discrete protein states. This suite of direct observations can be used to describe the statistical mechanical mechanisms of how proteins function, complete with fluctuation dynamics describing the kinetic rates between discrete states. (Lu et al., 1998; Rollins et al., 2014; Schuler et al., 2002; Yang et al., 2003).

Membrane proteins are of particular interest in neuroscience and can be more easily studied by single molecule fluorescence techniques than proteins that diffuse freely in all three dimensions. (Harms et al., 2003; Owen et al., 2012; Wang et al., 2014) Discussed in this article are a few examples of membrane bound proteins that act either as ion channels or enzymes, all of which can

* Corresponding author.

E-mail address: brozik@wsu.edu (J.A. Brozik).

be described as complex molecular machines with moving parts and two-dimensional lateral motions. A stochastic model can be used to describe the operation of molecular machines, which links allosteric motions and chemical reactions to changes in free energy. (Elber and Karplus, 1987; Jülicher and Bruinsma, 1998; Keller and Bustamante, 2014; Kurzynski and Chelminiak, 2014; Lazaridis and Karplus, 1999; Tsai, 2008) Such descriptions include the following phenomena: the closing of ligand binding clefts, (McCammon et al., 1976) rotations of subdomains, (De Groot et al., 1998; Noji et al., 1997) twisting of subunits, binding and unbinding of ligands, (Ghanouni et al., 2001; Lau and Roux, 2007; Ma et al., 2000; Ravindranathan et al., 2005) the metabolism of substrates (enzymes), (Rout et al., 2014) and the movement of proteins through lipid domains. (Wang et al., 2014) Each machine has a small number of key conformational degrees of freedom linked to these motions and chemical reactions, which result in the observable functional states (discrete states) of the protein. (Cooper, 1976; Kim, 2002a, 2002b; Thomas, 1996; Weiss, 2000) These motions and states are controlled by an underlying potential energy surface. (Best and Yng-Gwei, 2005) This surface is a function of the key conformational coordinates and interactions between the protein and the lipid membrane, all of which gives the free energy of each important functional state within specific microenvironments (domains). (Chou, 2001; Maddox, 2002) The local energy minima on this surface represent the discrete biochemical states that can, in principle, be observed at the single protein level. Hence, experimentally measured free energy differences between biochemical states tell us about the contours of the potential energy surface and the mechanisms that drive their properties. New single molecule experiments that allow for the direct observation of the functioning and interactions of membrane bound proteins (e.g. receptors, ion channels, membrane bound enzymes, etc.) will no doubt lead to paradigm shifts in our understanding of how such molecular machines work. (Yudowski et al., 2007).

1.2. Technical overview

Our current understanding of membrane proteins comes primarily from two types of information: structural information, which is mainly derived from x-ray crystallography and dynamical information from ensemble kinetic experiments. Though structural information describes how proteins are built and could, in principle at least, be used to predict dynamical information, direct measurement of kinetics is more practical. Connecting kinetic and thermodynamic properties to structure is a major goal in single molecule biophysics and great effort has been made to push techniques to higher spatial resolution (structure) (Rust et al., 2006) and ever faster time resolution (kinetics). (English et al., 2006; Turunen et al., 2014).

With regard to improvements in spatial resolution in particular, there are several well-established super-resolution single molecule fluorescence imaging techniques capable of resolving fluorescent emitters separated on the order of tens of nanometers (i.e. PALM, (Betzig et al., 2006) FPALM, (Hess et al., 2006) STORM, (Rust et al., 2006) dSTORM, (Heilemann et al., 2008) STED (Hell and Wichmann, 1994; Klar and Stefan, 1999), etc). The reader is referred to some of the many good reviews on the subject. (Coltharp et al., 2014; Henriques et al., 2011; Orrit et al., 2014; Patterson et al., 2010; Tonnesen and Nagerl, 2013) The term 'super-resolution' has evolved to mean that the image generated by the experiment has higher resolution than the diffraction limit of the microscope. Many super-resolution techniques use a form of stochastic reconstruction to build images with resolution accuracies that are ~10–100 times better than conventional fluorescence microscopy. All stochastic super-resolution techniques are

based on the same two-step process: super-localization (Thompson et al., 2002) followed by reconstruction. Super-localization forms the basis of single protein tracking and with the advent of fast highly sensitive EMCCD cameras and new fluorescent probe designs it is now possible to construct time-lapse super-resolution images on the ms time scale. This makes it possible to track membrane protein motion and biochemistry with spatial resolution well beyond the diffraction limit.

The diffraction limit, d , of a conventional fluorescence microscope in the x,y-plane is given by Abbe's formula: $d = \lambda/2NA$ where λ is the wavelength of the fluorescence and NA is the numerical aperture of the microscope objective. (Abbe, 1873) Using Abbe's formula, it can be shown that the typical diffraction limit is ~200 nm when using modern high NA objectives (1.4–1.45) and fluorophores like Cy3. As a reference, most small organic fluorophores are ~1 nm, commercially available quantum dots range from ~10 to 20 nm (LifeTechnologies™), and fluorescent proteins are ~3–4 nm (GFP). (Yang et al., 1996) Because of their small size, all will give rise to a diffraction limited spot with a full width at half maximum (FWHM) of ~200 nm (the diffraction limit). But since the emitted photons are a sampling of a fluorophore's true position, the location of the emitter can be determined with low nanometer precision by determining the peak of this distribution. The peak of the distribution is determined by fitting it to a point spread function (PSF; an Airy function or 2D-Gaussian) and the localization precision of the fluorophore (in the x,y-plane) is estimated from the Thompson–Larsen–Webb equation below:

$$\sigma_{xy} = \left[\left(\frac{s_i^2}{N} \right) + \frac{a^2}{12N} + \frac{8\pi s_i^4 b}{a^2 N^2} \right]^{\frac{1}{2}}$$

where σ_{xy} is the standard error of the mean (SEM) from a single point emitter, s_i is the standard deviation of the Gaussian distribution that equals $(2.2)^{-1}$ of the PSF width, a is the pixel size, b is the background, and N is the number of photons collected. (Thompson et al., 2002) In general, this type of analysis is called super-localization and the reconstruction of an image based on super-localization data produces a super-resolution image. The ability to carry out a time sequence of super localization measurements or super-resolution images is the essential step needed to carry out single protein tracking experiments used to determine elementary kinetic rates associated with discrete mechanistic states.

1.3. Super resolution imaging and tracking of individual membrane proteins

Most stochastic super-resolution techniques like STORM, dSTORM, PALM, FPALM, and their many variants are primarily used to image densely packed biological structures including: mitochondria, (Shim et al., 2012) other organelles, synapses, (Dani et al., 2010) large membrane 'patches,' viruses, and whole cells with a lateral resolution of ~20 nm and an axial resolution of ~50 nm. (Juetter et al., 2008; Nickerson et al., 2014) These techniques involve the use of large numbers of photo-switchable or photoactivatable fluorescent probe molecules (STORM) or fluorescence proteins (PALM) to specifically label a protein structure(s). This provides contrast to the fluorescent image and gives fundamental details about its biochemical make-up. The fluorophores are then activated with a laser pulse to stochastically 'turn on'—make fluorescent—a small spatially separated subset of these probes, which are excited by a second laser, and appear as diffraction limited spots on a camera. This process is repeated many times storing each image separately. After data collection is complete, the super-localization

of each spot is determined and a static super-resolution image is reconstructed.

In contrast, single protein tracking uses the same principles of super-localization but instead follows the sequential motions and chemistry of individual proteins in the time domain. (Manley et al., 2008) Protein machines are probabilistic by their very nature and they 'diffuse' stochastically between discrete biochemical states, which are the minima of their potential energy surfaces. (Fujiwara et al., 2002; Poudel, 2011, 2012) It should be noted that the potential energy surface is a function of many variables including the structure of the protein and its microenvironment. Therefore the stochastics are inherent to the proteins themselves and carry mechanistic as well as spatial and kinetic information. Instead of building up a static super-resolution spatial image, single protein tracking can be used to build up a dynamic super-resolution 'image' of the potential energy surface. Such information describes how chemistry and motion couple to change the free energy landscape, thus providing insight into a protein's biochemical mechanism. This article will demonstrate how single protein tracking can be used to provide some of the essential elements needed to experimentally explore potential energy surfaces.

2. Definitions

Lipids: 1,2-dimyristoyl-sn-glycero-3-phosphocholine (DMPC), 1- α -lysophosphatidyl-serine (Brain-PS), 1,2-dioleoyl-sn-glycero-3-phosphoethanolamine-N-[methoxy(poly-ethyleneglycol)-2000] (ammonium salt) (PEG-PE), 1,2-dioleoyl-sn-glycero-3-phosphocholine (DOPC), 1,2-dilauroyl-sn-glycero-3-phosphocholine (DLPC), 1,2-dilauroyl-sn-glycero-3-phospho-L-serine (DLPS), dihexadecyldimethylammonium bromide (DHADAB).

3. Ligand binding dynamics and stoichiometry

For membrane proteins such as ligand gated ion channels (LGIC) the binding and unbinding of small molecules provides the 'fuel' or 'ratchet' that drives the protein machine forward. (Lemoine et al., 2012) The discrete binding states of these ligands are often associated with minima in the potential energy surface corresponding to the proteins' conformational states. (Boehr et al., 2009; Niesen et al., 2011) The section below describes two examples of how single molecule tracking can be used to follow ligand binding in two different membrane protein systems. Such measurements can be used to ascertain elementary kinetic rate constants, micro- K_d 's, and stochastically describe stoichiometry.

These elements form the basis necessary to build a discrete state mechanistic model from which other single molecule experiments can be designed to probe.

Traditional kinetic experiments probe the dynamics associated with large ensembles after an external stimulation. The external stimulus (i.e. addition of a ligands, fast washing, externally applied voltage, etc.) will bring a system out of equilibrium and the dynamics are probed during relaxation back to equilibrium or as it reaches a new equilibrium. (McQuarrie and Simon, 1997) By contrast, in single molecule kinetic experiments involving membrane proteins there is no need to bring the system out of equilibrium. (Shi et al., 2008) Instead the elementary kinetic rate constants can be determined by following the fluctuation dynamics of individual membrane proteins. (Selvin and Ha, 2008).

In this special addition of Neuropharmacology, Ruepp et al. (2015) present ensemble measurements of binding of a fluorescent analog of ATP (Alexa-647-ATP, or ATP*) at the purinergic receptor P2X1. Single molecule binding studies provide complimentary information for ATP* binding, revealing a strong binding state at short times. The short time resolution afforded by single molecule experiments is not attainable from the rapid washing experiments of Ruepp et al. (2015) and therefore is complimentary to their ensemble studies.

The details of the single molecule P2X1 studies are given as [supplementary information](#). Briefly, purified P2X1 receptors were reconstituted in liposomes containing DMPC and PEG-PE and allowed to form lipid bilayers on hydrophilically treated borosilicate glass coverslips. DMPC/PEG-PE form a homogeneous lipid bilayer and at the experimental temperature (10 °C) is in a highly ordered L_β phase which immobilizes the P2X1 receptors in the membrane. (Poudel et al., 2012) In this way, individual P2X1 receptors are identified by their spatial location which was measured with ~10 nm precision. The unbinding of ATP* from individual P2X1 receptors can be followed over a long period of time (~1hr). Bright spots are attributed to ATP* being bound to P2X1 receptors. Therefore, the rate of going from light to dark is the ligand dissociation rate. From only 776 individually monitored P2X1 proteins, 445,882 individual dissociation rates were measured. [Fig. 1A](#) depicts a time trace of ATP* interacting with a single P2X1 protein. In this experiment, a signal above the dotted line is attributed to a state in which ATP* is bound to the P2X1 receptor. At the 10 s fiducial mark the P2X1 receptor is unbound, at ~15 s an ATP* binds to P2X1 receptor for 1.7 s before it unbinds, then an ATP* again binds to the P2X1 receptor for 4.1 s before it unbinds, etc. A histogram of all the 'on times' gives a probability distribution for ATP*

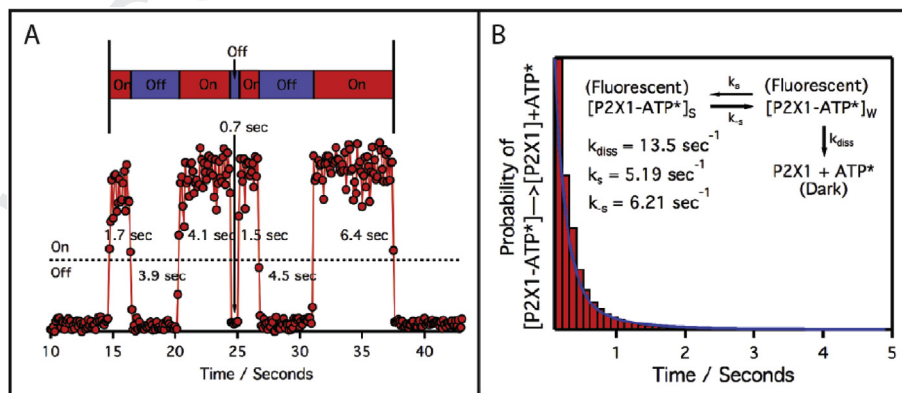


Fig. 1. (A) Single molecule time trace of individual ATP*s binding to a single spatially localized P2X1 receptor. The receptor was inserted into a DMPC/PEG-PE/Brain-PS biomimetic assembly on hydrophilically treated glass and cooled to 10 °C; past its L_β phase transition temperature. (B) Probability distribution for the dissociation of ATP* from P2X1 receptors. The distribution is a histogram of 445,882 individual residence times of single ATP*s bound 776 individually monitored P2X1 proteins. The data was numerically fit to a dissociation model that invoked a strong and weak binding state. (Original data).

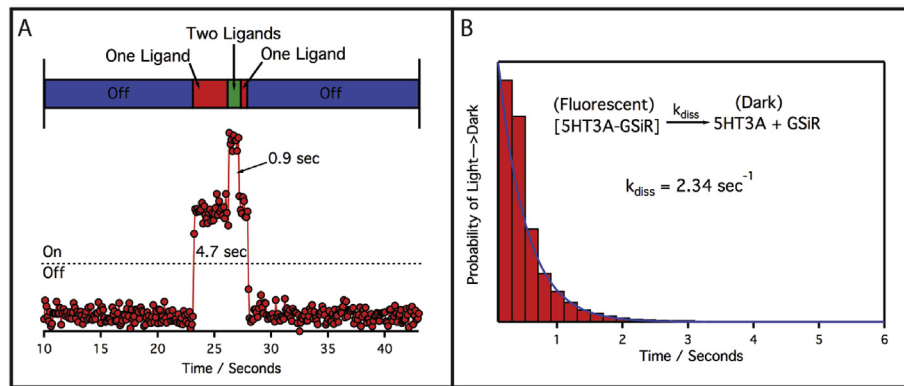


Fig. 2. (A) Single molecule time trace of individual Gr-SiRs binding to a single spatially localized 5HT_{3A} receptor. The receptor was inserted into a DMPC/PEG-PE/Brain-PS biomimetic assembly on hydrophilically treated glass and cooled to 10 °C; past its L_p' phase transition temperature. The bar above the figure indicates when a single ligand is bound to the receptor, when two ligands are bound, and when none are bound. This type of time trace occurs in ~3% of the measured time traces. (B) Probability distribution for the dissociation of G-SiR from 5HT_{3A}. The distribution is a histogram of Gr-SiR residence times on individual 5HT_{3A} receptors. Data was fit to a first order integrated rate law. (Original data).

dissociation (Fig. 1B). The tail of the dissociation curve appears to be first order as seen by Ruepp et al. (2015) but when the full time course is examined the kinetics are not entirely first order. Data from the time traces show no indication that there is more than one ATP* binding to any one P2X1 receptor; the associated stoichiometry is 1:1 (ligand:receptor). Therefore, the simplest model that fits the data is one that invokes a strong and weak binding state of ATP* on the P2X1 receptor as indicated in Fig. 1B. A single exponential fit of the tail alone gives a $k_{\text{tail}} = 1.78 \text{ sec}^{-1}$, which is fast compared to the dissociation rates measured by Ruepp et al (2015) ($k_d = 0.136 \text{ sec}^{-1}$) but this is probably attributable to the different conditions of the two experiments (biomimetic vs. HEK293T cells).

As a second example, the homopentamer of the serotonin type-3 receptor (5HT_{3A}) was prepared in an identical fashion as the P2X1 receptor samples and the unbinding of a fluorescent analog of granisetron (Gr-SiR) (Jack et al., 2015) was followed by single molecule tracking as described above. The homopentamer 5HT_{3A} has five identical allosteric binding sites and granisetron is a 5HT₃ specific antagonist. While it is generally accepted that multiple serotonin molecules can bind to 5HT_{3A} simultaneously, (Corradi

et al., 2009; Jackson and Yakel, 1995; Silva-Lopez et al., 2012; Solt et al., 2007) it is unknown how many granisetron molecules can bind to an individual receptor. This is because competitive antagonists, like granisetron, don't produce a conformational change when bound to the 5HT_{3A} receptor and therefore don't produce a cooperative (or anti-cooperative) affinity toward multi-antagonist binding. Because of this, ensemble experiments cannot distinguish between a population of 5HT_{3A} receptors occupied by a single granisetron molecule and receptors occupied by granisetron at multiple sites. At the low concentrations of Gr-SiR used in our experiments, the dominant observation at the single molecule level is a 1:1 stoichiometry with a first order dissociation rate, indicating a simple dissociation mechanism as depicted in Fig. 2B. But the single molecule intensity time trace also reveals a minor component in which a second Gr-SiR will bind to a single 5HT_{3A} receptor in ~3% of the observed tracks. Fig. 3A is such a time trace associated with an individual 5HT_{3A} receptor. At the beginning of the track the receptor is in an unbound state, at 23.2 s the first Gr-SiR binds, then at 26.3 s a second Gr-SiR binds to the receptor, followed by stepwise dissociation of both ligands. Such behavior demonstrates,

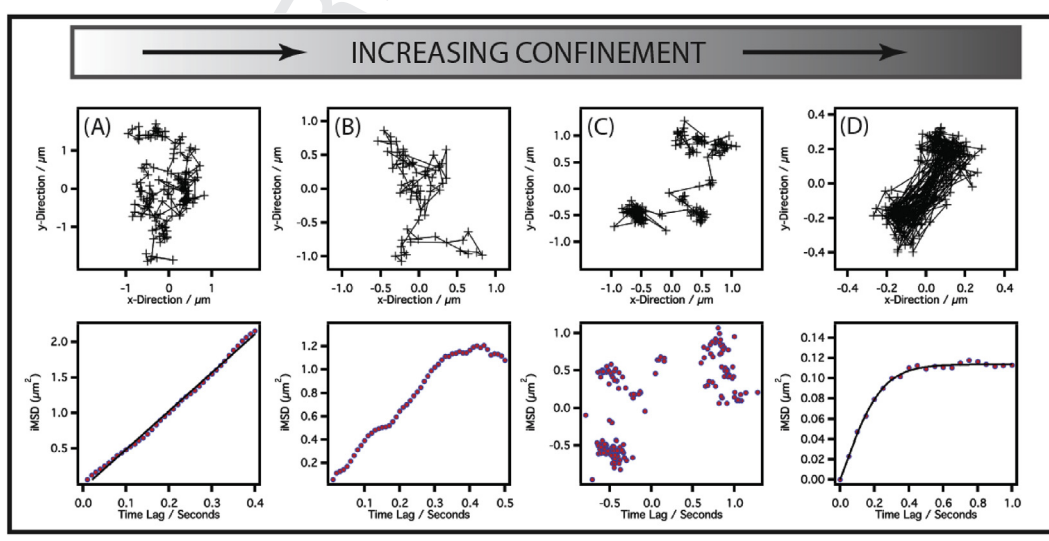


Fig. 3. Protein tracks (upper) and accompanying mean squared displacements vs. lag time (lower). (A) Example of normal diffusion from Poudel et al. (Poudel et al., 2012); Annexin V labeled with Alexa555 at 30 °C in a solid supported biomimetic membrane composed of DMPC/PEG-PE/Brain-PS. (B) Example hinder diffusion (original data). CPR labeled at a cysteine residue with Alexa555 at 30 °C in a solid supported biomimetic composed of DOPC/DLPC/DLPS. (C) Example of hop diffusion (original data). Same as (B) except at 17 °C. (D) Example of corralled diffusion from Poudel et al. (Poudel et al., 2011); 5-HT₃ labeled at its N-terminus with Alexa555 at 25 °C in a doubled cushioned bilayer composed of POPC/PEG-PE and corralled by BSA.

that for 5HT_{3A} and Gr-SiR, the fluctuation stoichiometry can be 2:1 (ligand:receptor) for brief periods of time, while the same behavior is yet to be observed in the P2X1 data at the concentrations tested.

These two examples demonstrate how the direct observation of fluctuation dynamics can reveal details that are not observable in bulk, but appear at the single molecule level. By simply counting, the statistical significance of these new observations can also be addressed. For example the strong and weak binding states of ATP* on P2X1 receptors are statistically significant. On the other hand, the second binding of Gr-SiR to 5HT_{3A} receptors is relatively rare in comparison to one bound ligand although it may be functionally significant. The importance is that all observables can be embedded into a more detailed discrete mechanism, which can be further studied by other single molecule methods.

4. Single protein tracking

The ways in which membrane proteins diffuse and are compartmentalized within a cell membrane are important elements of their overall function. Direct observation through single protein tracking has become an essential tool used to identify these motions and confinement. There are several modes of diffusion that are observed when tracking individual proteins in biological and biomimetic membranes. Though fundamentally Brownian, the different diffusion modes simply reflect the degree of confinement and mean free path experienced by the membrane protein within the two-dimensional plane of the biomimetic. In order of increasing confinement, and decreasing mean free path, these modes can be categorized as normal diffusion (free diffusion), hindered diffusion, hop diffusion, and corralled diffusion (confined diffusion). (Kusumi et al., 1993; Saxton and Jacobson, 1997) The ability to recognize these modes allows for a closer analysis of a membrane protein's microenvironment and is an essential part of any detailed pharmacokinetic model. (Pereira, 2010; Poudel et al., 2012; Sykes et al., 2014).

Like all single molecule work, there is extraordinary power in direct observation. More often than not, the dominant mode of diffusion can be determined by simply tracking the movement of a membrane protein. A single protein track is generated from a frame-to-frame analysis of super-localization data. In this analysis a fluorescently labeled protein is detected and identified by its super-localization as described above. The distance over which a protein is likely to move from one frame to the next is determined by its diffusion coefficient and degree of confinement. In order to track a membrane protein, an upper limit for the distance it can travel is set. If a diffraction limited fluorescent spot appears in the next frame and if that spot is under the maximally set limit, then it is attributed to the same protein. In this way the movement of individual proteins can be tracked.

Fig. 3 depicts a number of transmembrane proteins diffusing in biomimetic membranes with increasing amounts of confinement. At 30 °C, a membrane composed of DMPC, PEG-PE, and Brain-PS will form a homogeneous liquid-phase cushioned bilayer. At pH 6 and in the presence of 8 mM Ca²⁺, Annexin V adopts a transmembrane configuration and will diffuse in two dimensions. (Diaz et al., 2008) Because of the cushion formed by the PEG-PE, Annexin V experiences very little interaction with the underlying support and is free to diffuse in a nearly unconfined manner. (Poudel et al., 2012) The upper portion of Fig. 3A depicts a single protein track of Annexin V under these conditions and is a representative example of the type of diffusion that is exclusively observed at 30 °C. This is an example of unhindered Brownian diffusion at constant temperature, pressure and concentration and is characterized by the random nature of the track.

Normal diffusion can also be characterized by inspection of the individual mean squared displacement (iMSD) of the protein vs. lag time (Elliott et al., 2011; McCain et al., 2003; Poudel et al., 2013, 2011, 2012; Saxton, 1997; Saxton and Jacobson, 1997) The iMSD is derived from individual frame-to-frame squared displacements given by the equation below (Saxton and Jacobson, 1997):

$$(\Delta r_{n\Delta t})^2 = (\Delta x_{n\Delta t})^2 + (\Delta y_{n\Delta t})^2$$

where n is the frame number, Δt is the time between adjacent frames, and $\Delta x_{n\Delta t}$ and $\Delta y_{n\Delta t}$ are the spatial displacements in the x and y directions for time lag $n\Delta t$. The iMSD for the entire track is then given by:

$$\langle \Delta r_{n\Delta t}^2 \rangle = \frac{1}{N} \sum_{i=1}^N \Delta r_{i,n\Delta t}^2$$

where N is the total number of frames.

A normal Brownian diffuser is one that does not experience physical barriers or strong associations with immobile or slowly diffusing membrane components (i.e. lipid rafts or domains, anchoring proteins, underlying substrate, large protein complexes, etc.). A plot of its iMSD vs $n\Delta t$ will give a straight line in accordance with the Stokes–Einstein relation for two-dimensional diffusion given below:

$$\langle \Delta r_{n\Delta t}^2 \rangle = 4D(n\Delta t)$$

where D is the diffusion coefficient associated with the membrane protein. Inspection of the iMSD vs. lag time for Annexin V (lower portion of Fig. 3A) produces a linear relationship, but upon close inspection one does observe small undulations that are canceled out when an average MSD vs. lag time is plotted out (Poudel et al., 2012); $MSD = \sum iMSD_i$ where the sum is over all tracks. These small undulations are indicative of small deviations from 'normal diffusion'.

Because of the complexity of biological membranes and the design of most biomimetics, very few membrane proteins undergo normal diffusion. Instead of diffusing through a homogeneous liquid environment, they are constantly bumping into physical obstacles and temporarily binding with other membrane components. Depicted in Fig. 3B is a track of a membrane protein as it bumps into physical barriers setup in a biomimetic membrane. In this example, Cytochrome P450 Reductase (CPR) was fluorescently labeled at a solvent accessible cysteine in its cytosolic domain and inserted into a biomimetic membrane composed of DOPC, DLPC, and DLPS (1:1:1 by weight) at 25 °C; see supplementary information for experimental details. Under these experimental conditions, the membrane is quite heterogeneous and will form domains that are rich in PS containing lipids compared with the bulk membrane that is rich in PC containing lipids. As a result CPR will diffuse with a variety of different confined motions. The mode of diffusion depicted in Fig. 3B is a good example of hindered diffusion caused by heterogeneity in the microenvironment. By inspection of the single protein track it is apparent that the protein is not completely free to diffuse, but instead will follow an obstructed path through the membrane. More telling is the large undulations observed in the iMSD vs. $n\Delta t$ plot. Undulations are typically observed in tracks dominated by hindered diffusion.

As confinement increases, hindered diffusion will merge into what is commonly known as hop-diffusion. This begins to appear when more obstacles are present and the mean free path available to the protein is decreased. In this mode of diffusion the protein is

temporarily contained in small domains but can still escape and be temporarily trapped in an adjacent domain. The track depicted in Fig. 3C comes from the same data set in which 3B was obtained, the only difference is that the temperature was lowered from 30 °C to 17 °C causing more heterogeneity in the membrane and decreasing the mean free path of the protein. In this example, hopping from region-to-region is clearly observed. This also results in a scattered iMSD vs. $n\Delta t$ plot (Fig. 3C lower curve).

As confinement increases further, the mean free path available to the protein becomes limited to a small confined region, which will corral the protein. The protein is still free to diffuse in this region but cannot escape. Fig. 3D depicts a track from an individual 5-HT₃ receptor labeled at its N-terminus with Alexa555 and inserted into a cushioned membrane composed of POPC and PEG-PE on a support coated with Bovine Serum Albumen (BSA) at 25 °C. (Poudel et al., 2011) In this biomimetic system, the underlying BSA layer creates small corraling domains of varying shapes and ~100–400 nm in size. By inspection of the track 5-HT₃ makes, it is clear that it is corralled but can still diffuse within the corral. Inspection of the plot of iMSD vs. $n\Delta t$ shows a linear region followed by a plateau determined by the size of the corral. This mode of diffusion is well described by the approximate equation below:

$$\langle \Delta r_{n\Delta t}^2 \rangle \cong \langle r_c^2 \rangle \left[1 - A_1 \exp\left(\frac{-4A_2 D(n\Delta t)}{\langle r_c^2 \rangle}\right) \right]$$

where r_c^2 is the square of the average corral size, A_1 and A_2 reflect the shape of the corral, and D is the diffusion coefficient.

In summary, Fig. 3 gives clear examples of four main types of Brownian diffusion exhibited by proteins in membranes, but it should be noted that the level of confinement is best described as a continuum and the mode of diffusion will often fall somewhere in between the above stated categories. It is also typical to observe more than one type of motion in a single track, such as a membrane protein moving between two distinct compartments. Such things are common and important aspects of some biochemical mechanisms and membrane protein function. It is also noted that most membrane proteins will diffuse normally at very short time lags, that is, their iMSD will be linear. (Qian et al., 1991; Sako and Kusumi, 1994; Saxton and Jacobson, 1997) Finally, all membrane proteins are confined by the membrane or to a region of the membrane and will show corralled behavior at long enough time lags.

5. Chemical potential from single molecule tracking

Tracking the fluctuation kinetics (Section 3) and the mass transport properties (Section 4) associated with individual membrane proteins are key steps in establishing a discrete state mechanism. It establishes which are the most probable (longest lived) biochemical states, which are more transient, and what is the most probable sequence of going from one state to the next. It also can reveal hidden complexities associated with an observable state. Once a discrete state mechanism is established, much of the thermodynamics associated with that mechanism can be experimentally determined by identifying each biochemical state within the field of view and keeping track of their occurrence rates.

An instructive example comes from a single molecule tracking study of gramicidin in a biomimetic membrane composed of DMPC, DHADAB, and cholesterol. (Davis et al., 2004) Gramicidin is a simple sodium ion channel. Each gramicidin subunit consists of a single β -helix of only 15 amino acids. Subunits diffuse within this membrane and will stochastically form dimers. These dimers orient themselves perpendicular to the membrane and form Na⁺ channels. (Koeppel and Anderson, 1996; Urry et al., 1971; Woolley and Wallace, 1992) Davis et al. (Davis et al., 2004) labeled gramicidin subunits with Rhodamine-6G and identified the monomer and dimer states independently of one another. Since each individual subunit possessed a Rhodamine label, fluorescence from gramicidin dimers was more intense than from individual monomers. Moreover, dimers diffused more slowly than monomers because of their increased hydrodynamic cross section. Fig. 4A is a 3-D histogram correlating brightness with diffusion coefficients of individually tracked monomers and dimers of gramicidin. Two states are clearly identified; a bright slow state and a dim fast state. The bright slow state is attributed to the dimers and the dim fast state is attributed to monomers. Using this criterion to identify individual states, and then counting monomers vs. dimers, the equilibrium constant can be determined and the free energy is given by $\Delta G^0(T) = -RT \ln(K_{eq}(T))$. The equilibrium constant changes with temperature, and by using the van't Hoff equation, ΔH^0 was determined. Finally, ΔS^0 was determined from $\Delta G^0(T) = \Delta H^0 - T\Delta S^0$. In this way, all thermodynamic parameters associated with the minima in a potential energy surface can be determined by identifying the states, counting, and changing the temperature.

The above example is quite simple and provides a roadmap of how to experimentally determine a potential energy surface. After

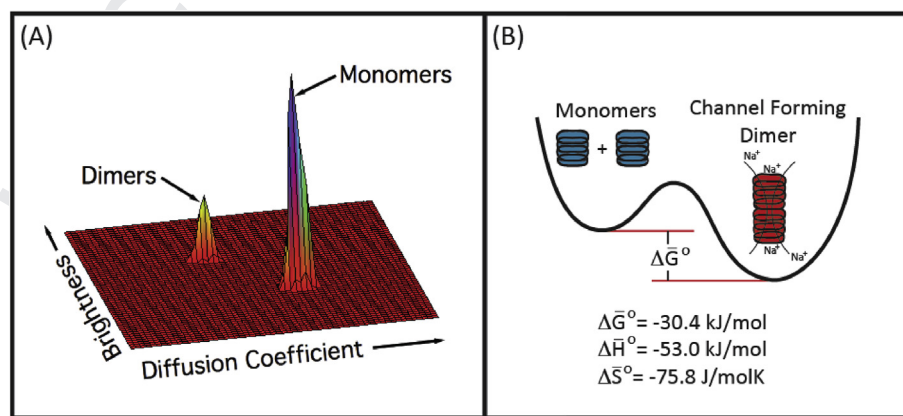


Fig. 4. (A) 3D histogram of gramicidin monomers and dimers. Along the x-axis is the brightness of the fluorescence intensity from individual gramicidin tracks, along the y-axis is the diffusion coefficient, and along the z-axis is the number of gramicidin tracks associated with the same values for brightness and diffusion coefficient. (B) Potential energy diagram for gramicidin monomer going to dimers. The values for ΔG^0 , ΔH^0 , and ΔS^0 are standard state values at 25 °C. Data from Davis et al. (Davis et al., 2004).

a detailed discrete state mechanism is established, a follow-up single molecule experiment can be designed to observe and identify individual biochemical states that are connected by an elementary step in the mechanism. Then all that is needed is to count up the number of occupancies in one state vs. another. That ratio (raised to corresponding stoichiometric coefficients) is the potential energy difference between adjacent mechanistic steps. By changing the temperature and making corresponding observations, all thermodynamic parameters associated with any particular step in the potential energy surface can be determined.

6. Super-resolution imaging of microenvironments

Biological membranes are crowded, complex places. They are packed with a variety of lipids, proteins, sugars, small molecules, cytoskeletal scaffolds, and many other components depending on what cells or organelles they are associated with. (Sezgin et al., 2014; Simons and Sampaio, 2011; van Meer et al., 2008; Zhou, 2009) As such, biological membranes are quite heterogeneous and form a mosaic of different chemical and physical phase domains. (Goñi, 2014; Harder et al., 1998; Lingwood and Simons, 2010; Singer and Nicolson, 1972) Membrane proteins are in intimate contact with these chemical components and phases and will often partition into a preferred domain. (Lemmon, 2008; Mbamala et al., 2005) How a protein is partitioned in a membrane is as much a part of its function and mechanism as its internal states and motions. (Domański et al., 2012; Simons and Ikonen, 1997) The domains in a biological or biomimetic membrane are small, ranging from 10 to 200 nm in a biological membrane and up to microns in a biomimetic. (Brown et al., 2007; de Almeida et al., 2005; Dietrich et al., 2001) The ability to directly observe a single membrane protein as it interacts with a heterogeneous lipid membrane adds new insight into how proteins work in tandem with their microenvironment. (Poudel et al., 2012; Poudel, 2011).

Consider the CPR protein and biomimetic systems described in Section 4. As mentioned above, the biomimetic is quite heterogeneous and will form PS enriched domains as depicted in Fig. 5. CPR can insert at the phase boundary between a PS rich domain and the bulk membrane. After insertion, CPR will diffuse in a pseudo-1D fashion (a ring) mapping out its microenvironment around the PS rich phase domain. The right side of Fig. 5 is a super-resolution image of a single CPR protein that was tracked for 9.87 s before the Alexa-555 label on the CPR irreversibly bleached. Each image is a snapshot of the CPR's location at 10 ms intervals; 987 individual images were collected. The super-localization at each time interval was determined as described in Section 1 and all 987 locations were used to reconstruct the super-resolution image in

Fig. 5. The reconstructed image shows a single CPR circumnavigating a domain that is at least 565 nm in diameter. It also shows that the movement of CPR is limited to a ring that is only 75 nm wide. This discovery is being used to suggest a new mechanism of how CPR transfers electrons to P450s in such heterogeneous environments and is an important example of why compartmentalization of proteins in membrane should be given careful consideration.

7. Conclusion

There are great scientific advantages in making direct observations associated with individual objects, versus ensemble measurements. Direct observations provide irrefutable evidence for the existence of something regardless of how common or rare it might be, whereas such behavior could be seen to 'average out' when ensemble measurements are made. The ability to make these observations in a time dependent fashion allows a scientist to deduce a sequence, which is intimately tied to a mechanism of action. As a discipline, biology has used this approach to deduce complex cause and effect relationships in nature. The ability to bring this approach down to the single protein level is also proving to be an important tool in biochemistry. But as the objects we study get smaller and smaller the laws governing their mechanisms of action begin to change. Instead of deterministic cause and effect relationships, the physics governing small protein machines—indeed of the entire microscopic world—are stochastic. Thus, observations made at the single protein level are statistical in nature. Every protein machine is a diffuser on a potential energy surface whose operation is ratcheted forward through the transduction of free energy into useful work. Such operations include the breaking and making of chemical bonds, interactions with the microenvironment, the binding and unbinding of ligands, electron transfer reactions, mass transport, partitioning and spatial rearrangement, etc.

Described here is a framework of (1) how to use single protein tracking to build detailed discrete state mechanisms based on fluctuation kinetics; (2) how single protein tracking can be used to gain information about a protein's mass transport properties; (3) how the identification and quantification of biochemical states on individual proteins can be used to determine chemical potential, enthalpy, and entropy; (4) and how super-resolution imaging can yield key information about compartmentalization of membrane proteins in complex heterogeneous environments. These approaches are currently being used to probe some of the key variables associated with the discrete states of protein molecular machines. As the techniques are pushed to ever greater spatial and temporal resolution, the rest will soon follow.

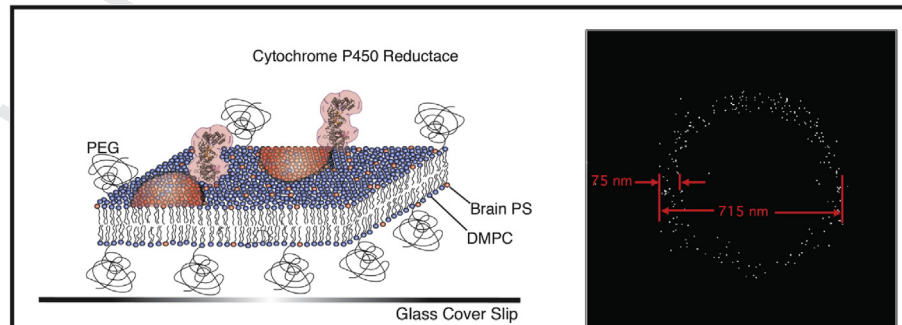


Fig. 5. Super resolution image of CPR in a DOPC/DLPC/DLPS biomimetic at 25 °C on a glass substrate (right). The sketch (left) is of the membrane with CPR inserted into a phase boundary between a PS rich domain and the bulk membrane rich in PC. (Original data).

Acknowledgments

Support to JAB was provided through the United States Air Force, Office of Scientific Research, Grant Number: FA9550-14-1-0272. AJT was funded by the British Heart Foundation (PG/13/39/30293).

Appendix A. Supplementary data

Supplementary data related to this article can be found at <http://dx.doi.org/10.1016/j.neuropharm.2015.05.003>.

References

- Abbe, E., 1873. Beiträge zur Theorie des Mikroskops und der mikroskopischen Wahrnehmung. *Arch. für Mikrosk. Anat.* 9, 413–418.
- Best, R.B., Yng-Gwei, C., 2005. Slow protein conformational dynamics from multiple experimental structures: the helix/sheet transition of arc repressor. *Structure* 13, 1755–1763.
- Betzig, E., Patterson, G.H., Sougrat, R., Lindwasser, O.W., Olenych, S., Bonifacio, J.S., Davidson, M.W., Lippincott-Schwartz, J., Hess, H.F., 2006. Imaging intracellular fluorescent proteins at nanometer resolution. *Science* 313, 1642–1645.
- Boehr, D.D., Nussinov, R., Wright, P.E., 2009. The role of dynamic conformational ensembles in biomolecular recognition. *Nat. Chem. Biol.* 5, 789–796.
- Brown, A.C., Towles, K.B., Wrenn, S.P., 2007. Measuring raft size as a function of membrane composition in PC-based systems: part II—ternary systems. *Langmuir* 23, 11188–11196.
- Chou, T.K., Ken, S., Oster, George, 2001. Statistical thermodynamics of membrane bending-mediated protein-protein attractions. *Biophys. J.* 80, 1075–1087.
- Coltharp, C., Yang, X., Xiao, J., 2014. Quantitative analysis of single-molecule superresolution images. *Curr. Opin. Struct. Biol.* 28c, 112–121.
- Cooper, A., 1976. Thermodynamic fluctuations in protein molecules. *Biochemistry* 73, 2740–2741.
- Corradi, J., Gumilar, F., Bouzat, C., 2009. Single-channel kinetic analysis for activation and desensitization of homomeric 5-HT_{3A} receptors. *Biophys. J.* 97, 1335–1345.
- Dani, A., Bo, H., Bergan, Joseph, Dulac, Catherine, Zhuang, Xiaowei, 2010. Super-resolution imaging of chemical synapses in the brain. *Neuron* 68, 843–856.
- Davis, R.W., Patrick, E.L., Meyer, L.A., Ortiz, T.P., Marshall, J.A., Keller, D.J., Brozik, S.M., Brozik, J.A., 2004. Thermodynamic properties of single ion channel formation: gramicidin. *J. Phys. Chem. B* 108, 15364–15369.
- de Almeida, R.F.M., Loura, L.M.S., Fedorov, A., Prieto, M., 2005. Lipid rafts have different sizes depending on membrane composition: a time-resolved fluorescence resonance energy transfer study. *J. Mol. Biol.* 346, 1109–1120.
- De Groot, B., Hayward, S., Van Aalten, D., Amadei, A., Berendsen, H., 1998. Domain motions in bacteriophage T4 lysozyme: a comparison between molecular dynamics and crystallographic data. *Proteins Struct. Funct. Genet.* 31, 116–127.
- Diaz, A.J., Albertorio, F., Daniel, S., Cremer, P.S., 2008. Double cushions preserve transmembrane protein mobility in supported bilayer systems. *Langmuir* 24, 6820–6826.
- Dietrich, C., Bagatolli, L.A., Volovyk, Z.N., Thompson, N.L., Levi, M., Jacobson, K., Gratton, E., 2001. Lipid rafts reconstituted in model membranes. *Biophys. J.* 80, 1417–1428.
- Domański, J., Marrink, S.J., Schäfer, L.V., 2012. Transmembrane helices can induce domain formation in crowded model membranes. *Biochim. Biophys. Acta (BBA) – Biomembr.* 1818, 984–994.
- Elber, R., Karplus, M., 1987. Multiple conformational states of proteins: a molecular dynamics analysis of myoglobin. *Science* 235, 318–321.
- Elliott, L.C.C., Barhoum, M., Harris, J.M., Bohn, P.W., 2011. Trajectory analysis of single molecules exhibiting non-Brownian motion. *Phys. Chem. Chem. Phys.* 13, 4326–4334.
- English, B.P., Wei, M., van Oijen, A.M., Kang Taek, L., Luo, G., Hongye, S., Cherayil, B.J., Kou, S.C., Xie, X.S., 2006. Ever-fluctuating single enzyme molecules: Michaelis-Menten equation revisited. *Nat. Chem. Biol.* 2, 87–94.
- Fujiwara, T., Ritchie, K., Murakoshi, H., Jacobson, K., Kusumi, A., 2002. Phospholipids undergo hop diffusion in compartmentalized cell membrane. *J. Cell Biol.* 157, 1071–1082.
- Ghanouni, P., Gryczynski, Z., Steenhuis, J.J., Lee, T.W., Farrens, D.L., Lakowicz, J.R., Kobilka, B.K., 2001. Functionally different agonists induce distinct conformations in the G Protein coupling domain of the β_2 adrenergic receptor. *J. Biol. Chem.* 276, 24433–24436.
- Goni, F.M., 2014. The basic structure and dynamics of cell membranes: an update of the singer–Nicolson model. *Biochim. Biophys. Acta (BBA) – Biomembr.* 1838, 1467–1476.
- Harder, T., Scheffele, P., Verkade, P., Simons, K., 1998. Lipid domain structure of the plasma membrane revealed by patching of membrane components. *J. Cell Biol.* 141, 929–942.
- Harms, G.S., Orr, G., Montal, M., Thrall, B.D., Colson, S.D., Lu, H.P., 2003. Probing conformational changes of gramicidin ion channels by single-molecule patch-clamp fluorescence microscopy. *Biophys. J.* 85, 1826–1838.

- Heilemann, M., van de Linde, S., Schüttel, M., Kasper, R., Seefeldt, B., Mukherjee, A., Tinnefeld, P., Sauer, M., 2008. Subdiffraction-resolution fluorescence imaging with conventional fluorescent probes. *Angew. Chem. Int. Ed.* 47, 6172–6176.
- Hell, S.W., Wichmann, J., 1994. Breaking the diffraction resolution limit by stimulated emission: stimulated-emission-depletion fluorescence microscopy. *Opt. Lett.* 19, 780–782.
- Henriques, R., Griffiths, C., Hesper Rego, E., Mhlana, M.M., 2011. PALM and STORM: unlocking live-cell super-resolution. *Biopolymers* 95, 322–331.
- Hess, S.T., Girirajan, T.P.K., Mason, M.D., 2006. Ultra-high resolution imaging by fluorescence photoactivation localization microscopy. *Biophys. J.* 91, 4258–4272.
- Jack, T., Simonin, J., Ruepp, M.D., Thompson, A.J., Gertsch, J., Lochner, M., 2015. Characterizing new fluorescent tools for studying 5-HT₃ receptor pharmacology. *Neuropharmacology* 90, 63–73.
- Jackson, M.B., Yakel, J.L., 1995. The 5-HT₃ receptor channel. *Annu. Rev. Physiol.* 447–468.
- Juette, M.F., Gould, T.J., Lessard, M.D., Mlodzianowski, M.J., Nagpure, B.S., Bennett, B.T., Hess, S.T., Bewersdorf, J., 2008. Three-dimensional sub-100 nm resolution fluorescence microscopy of thick samples. *Nat. Meth.* 5, 527–529.
- Jülicher, F., Bruinsma, R., 1998. Motion of RNA polymerase along DNA: a stochastic model. *Biophys. J.* 74, 1169–1185.
- Keller, D., Bustamante, C., 2014. The mechanochemistry of molecular motors. *Biophys. J.* 78, 541–556.
- Kim, M.K.C., Gregory, S., Jernigan, Robert L., 2002a. Elastic models of conformational transitions in macromolecules. *J. Mol. Graph. Model.* 21, 151–160.
- Kim, M.K.J., Robert, L., Chirikjian, Gregory S., 2002b. Efficient generation of feasible pathways for protein conformational transitions. *Biophys. J.* 83, 1620–1630.
- Klar, T.A., Stefan, W., 1999. Subdiffraction resolution in far-field fluorescence microscopy. *Opt. Lett.* 24, 954–956.
- Koeppel, R.E., Anderson, O.S., 1996. Engineering the gramicidin channel. *Annu. Rev. Biophys. Biomol. Struct.* 25, 231–258.
- Kurzynski, M., Chelminiak, P., 2014. Stochastic dynamics of proteins and the action of biological molecular machines. *Entropy* 16, 1969–1982.
- Kusumi, A., Sako, Y., Yamamoto, M., 1993. Confined lateral diffusion of membrane receptors as studied by single particle tracking (nanovid microscopy). Effects of calcium-induced differentiation in cultured epithelial cells. *Biophys. J.* 65, 2021–2040.
- Lau, A.Y., Roux, B., 2007. The free energy landscapes governing conformational changes in a glutamate receptor ligand-binding domain. *Structure* 15, 1203–1214.
- Lazaridis, T., Karplus, M., 1999. Effective energy function for proteins in solution. *Proteins: Struct. Funct. Bioinforma.* 35, 133–152.
- Lemmon, M.A., 2008. Membrane recognition by phospholipid-binding domains. *Nat. Rev. Mol. Cell. Biol.* 9, 99–111.
- Lemoine, D., Jiang, R., Taly, A., Chataigneau, T., Specht, A., Grutter, T., 2012. Ligand-gated ion channels: new insights into neurological disorders and ligand recognition. *Chem. Rev.* 112, 6285–6318.
- Lingwood, D., Simons, K., 2010. Lipid rafts as a membrane-organizing principle. *Science* 327, 46–50.
- Lu, H.P., Xun, L., Xie, X.S., 1998. Single-molecule enzymatic dynamics. *Science* 282, 1877–1882.
- Ma, J., Sigler, P.B., Xu, Z., Karplus, M., 2000. A dynamic model for the allosteric mechanism of GroEL. *J. Mol. Biol.* 302, 303–313.
- Maddox, M.W.L., Marjorie, L., 2002. A Monte Carlo study of peptide insertion into lipid bilayers: equilibrium conformations and insertion mechanisms. *Biophys. J.* 82, 244–263.
- Manley, S., Gillette, J.M., Patterson, G.H., Shroff, H., Hess, H.F., Betzig, E., Lippincott-Schwartz, J., 2008. High-density mapping of single-molecule trajectories with photoactivated localization microscopy. *Nat. Methods* 5, 155–157.
- Mbamala, E.C., Ben-Shaul, A., May, S., 2005. Domain formation induced by the adsorption of charged proteins on mixed lipid membranes. *Biophys. J.* 88, 1702–1714.
- McCain, K.S., Hanley, D.C., Harris, J.M., 2003. Single-molecule fluorescence trajectories for investigating molecular transport in thin silica sol–gel films. *Anal. Chem.* 75, 4351–4359.
- McCammon, J.A., Gelin, B.R., Karplus, M., Wolynes, P.G., 1976. The hinge-bending mode in lysozyme. *Nature* 262, 325–326.
- McQuarrie, D.A., Simon, J.D., 1997. *Physical Chemistry: a Molecular Approach*. University Science Books, Sausalito, Calif.
- Nickerson, A., Huang, T., Lin, L.-J., Nan, X., 2014. Photoactivated localization microscopy with bimolecular fluorescence complementation (BiFC-PALM) for nanoscale imaging of protein-protein interactions in cells. *PLoS One* 9, e100589.
- Niesen, M.J.M., Bhattacharya, S., Vaidehi, N., 2011. The role of conformational ensembles in ligand recognition in g-protein coupled receptors. *J. Amer. Chem. Soc.* 133, 13197–13204.
- Noji, H., Yasuda, R., Yoshida, M., Kinosita, K., 1997. Direct observation of the rotation of F1-ATPase. *Nature* 386, 299–302.
- Orrit, M., Ha, T., Sandoghdar, V., 2014. Single-molecule optical spectroscopy. *Chem. Soc. Rev.* 43, 973–976.
- Owen, D.M., Williamson, D.J., Magenau, A., Gaus, K., 2012. Sub-resolution lipid domains exist in the plasma membrane and regulate protein diffusion and distribution. *Nat. Commun.* 3, 1256.
- Patterson, G., Davidson, M., Manley, S., Lippincott-Schwartz, J., 2010. Super-resolution imaging using single-molecule localization. *Annu. Rev. Phys. Chem.* 61, 345–367.

- Pereira, L.M., 2010. Fractal pharmacokinetics. *Comput Math. Methods Med.* 11, 161–184.
- Poudel, K.R., Jones, J.P., Brozik, J.A., 2013. A guide to tracking single transmembrane proteins in supported lipid bilayers. *Methods Mol. Biol. (N. Y., N. Y. U. S.)* 974, 233–252.
- Poudel, K.R., Keller, D.J., Brozik, J.A., 2011a. Single particle tracking reveals corraling of a transmembrane protein in a double-cushioned lipid bilayer assembly. *Langmuir* 27, 320–327.
- Poudel, K.R.K., David, J., Brozik, James A., 2011b. Single particle tracking reveals corraling of a transmembrane protein in a double-cushioned lipid bilayer assembly. *Langmuir* 21, 320–327.
- Poudel, K.R.K., David, J., Brozik, James A., 2012. The effect of a phase transition on single molecule tracks of annexin V in cushioned DMPC assemblies. *Soft Matter* 8, 11285–11293.
- Qian, H., Sheetz, M.P., Elson, E.L., 1991. Single particle tracking. Analysis of diffusion and flow in two-dimensional systems. *Biophys. J.* 60, 910–921.
- Ravindranathan, K.P., Gallicchio, E., Levy, R.M., 2005. Conformational equilibria and free energy profiles for the allosteric transition of the ribose-binding protein. *J. Mol. Biol.* 353, 196–210.
- Rollins, G.C., Shin, J.Y., Bustamante, C., Presse, S., 2014. Stochastic approach to the molecular counting problem in superresolution microscopy. *Proc. Natl. Acad. Sci. U. S. A.*
- Rout, M.K., Hodge, C.D., Markin, C.J., Xu, X., Glover, J.N.M., Xiao, W., Spyropoulos, L., 2014. Stochastic gate dynamics regulate the catalytic activity of ubiquitination enzymes. *J. Am. Chem. Soc.* 136, 17446–17458.
- Rust, M.J., Bates, M., Zhuang, X., 2006. Sub-diffraction-limit imaging by stochastic optical reconstruction microscopy (STORM). *Nat. Methods* 3, 793–796.
- Sako, Y., Kusumi, A., 1994. Compartmentalized structure of the plasma membrane for receptor movements as revealed by a nanometer-level motion analysis. *J. Cell Biol.* 125, 1251–1264.
- Saxton, M.J., 1997. Single-particle tracking: the distribution of diffusion coefficients. *Biophys. J.* 72, 1744–1753.
- Saxton, M.J., Jacobson, K., 1997. Single-particle tracking: applications to membrane dynamics. *Annu. Rev. Biophys. Biomol. Struct.* 26, 373–399.
- Schuler, B., Lipman, E.A., Eaton, W.A., 2002. Probing the free-energy surface for protein folding with single-molecule fluorescence spectroscopy. *Nature* 419, 743–747.
- Selvin, P.R., Ha, T., 2008. *Single-molecule Techniques: a Laboratory Manual*. Cold Spring Harbor Laboratory Press.
- Sezgin, E., Sadowski, T., Simons, K., 2014. Measuring lipid packing of model and cellular membranes with environment sensitive probes. *Langmuir* 30, 8160–8166.
- Shi, J., Dertouzos, J., Gafni, A., Steel, D., 2008. Application of single-molecule spectroscopy in studying enzyme kinetics and mechanism. *Methods Enzym.* 450, 129–157.
- Shim, S.-H.X., Chenglong, Zhong, Guisheng, Babcock, Hazen P., Vaughan, Joshua C., Huang, Bo, Wang, Xun, Xu, Cheng, Bi, Guo-Qiang, Zhuang, Xiaowei, 2012. Super-resolution fluorescence imaging of organelles in live cells with photoswitchable membrane probes. *Proc. Natl. Acad. Sci. U. S. A.* 109, 13978–13983.
- Silva-Lopez, E.I., Barden, A.O., Brozik, J.A., 2012. Near native binding of a fluorescent serotonin conjugate to serotonin type 3 receptors. *Bioorg. Med. Chem. Lett.* 23, 773–775.
- Simons, K., Ikonen, E., 1997. Functional rafts in cell membranes. *Nature* 387, 569–572.
- Simons, K., Sampaio, J.L., 2011. Membrane organization and lipid rafts. *Cold Spring Harb. Perspect. Biol.* 3.
- Singer, S.J., Nicolson, G.L., 1972. The fluid mosaic model of the structure of cell membranes. *Science* 175, 720–731.
- Solt, K., Ruesch, D., Forman, S.A., Davies, P.A., Raines, D.E., 2007. Differential effects of serotonin and dopamine on human 5-HT_{3A} receptor kinetics: interpretation within an allosteric kinetic model. *J. Neurosci.* 27, 13151–13160.
- Sykes, D.A., Parry, C., Reilly, J., Wright, P., Fairhurst, R.A., Charlton, S.J., 2014. Observed drug-receptor association rates are governed by membrane affinity: the importance of establishing micro-pharmacokinetic/pharmacodynamic relationships at the β_2 -adrenoceptor. *Mol. Pharmacol.* 85, 608–617.
- Thomas, A.F., Martin, J., Mouawad, Liliane, Perahia, David, 1996. Analysis of the low frequency normal modes of the T-state of aspartate transcarbamylase. *J. Mol. Biol.* 257, 1070–1087.
- Thompson, R.E., Larson, Daniel R., Webb, Watt W., 2002. Precise nanometer localization analysis for individual fluorescent probes. *Biophys. J.* 82, 2775–2783.
- Tonnesen, J., Nagerl, U.V., 2013. Superresolution imaging for neuroscience. *Exp. Neurol.* 242, 33–40.
- Tsai, C.-J., Antonio, d. S., Nassinov, Ruth, 2008. Allostery: absence of a change in shape does not imply that allostery is not at play. *J. Mol. Biol.* 378, 1–11.
- Turunen, P., Rowan, A.E., Blank, K., 2014. Single-enzyme kinetics with fluorogenic substrates: lessons learnt and future directions. *FEBS Lett.* 588, 3553–3563.
- Urry, D.W., Goodall, M.C., Glickson, J.D., Mayers, D.F., 1971. The gramicidin A transmembrane channel: characteristics of head-to-head dimerized (LD) helices. *Proc. Natl. Acad. Sci. U. S. A.* 68, 1907–1911.
- van Meer, G., Voelker, D.R., Feigenson, G.W., 2008. Membrane lipids: where they are and how they behave. *Nat. Rev. Mol. Cell. Biol.* 9, 112–124.
- Wang, Y., Gao, J., Guo, X., Tong, T., Shi, X., Li, L., Qi, M., Wang, Y., Cai, M., Jiang, J., Xu, C., Ji, H., Wang, H., 2014. Regulation of EGFR nanocluster formation by ionic protein-lipid interaction. *Cell. Res.* 24, 959–976.
- Weiss, S., 2000. Measuring conformational dynamics of biomolecules by single molecule fluorescence spectroscopy. *Nat. Struct. Biol.* 7, 724–729.
- Woolley, G.A., Wallace, B.A., 1992. Model ion channels: gramicidin and alamethicin. *J. Membr. Biol.* 129, 109–136.
- Yang, F.M., Larry, G., Phillips, George N., 1996. The molecular structure of green fluorescent protein. *Nat. Biotechnol.* 14, 1246–1251.
- Yang, H., Luo, G., Karnchanaphanurach, P., Louie, T.-M., Rech, I., Cova, S., Xun, L., Xie, X.S., 2003. Protein conformational dynamics probed by single-molecule electron transfer. *Science* 302, 262–266.
- Yudowski, G.A.P., Manojkumar, A., Leonoudakis, Dmitri, Panicker, Sandip, Thorn, Kurt S., Beattie, Eric C., Zastrow, Mark von, 2007. Real-time imaging of discrete exocytic events mediating surface delivery of AMPA receptors. *J. Neurosci.* 27, 11112–11121.
- Zhou, H.-X., 2009. Crowding effects of membrane proteins. *J. Phys. Chem. B* 113, 7995–8005.